IEEE Access
Multidisciplinary | Rapid Review | Open Access Journal

Received September 9, 2021, accepted September 23, 2021, date of publication September 27, 2021,
date of current version October 6, 2021.

Digital Object Identifier 10.1109/ACCESS.2021.3115762

A Microwave Power Transmission System Using Sequential Phase Ring Antenna and Inverted Class F Rectenna

DANH MANH NGUYEN, (Student Member, IEEE), NGOC DUC AU, (Member, IEEE), AND CHULHUN SEO, (Senior Member, IEEE)

Department of Information and Communication Convergence, Soongsil University, Dongjak-gu, Seoul 06978, South Korea

Corresponding author: Chulhun Seo (chulhun@ssu.ac.kr)

This work was supported by the Basic Science Research Program through the National Research Foundation of Korea (NRF) by the Ministry of Science and ICT under Grant NRF-2017R1A5A1015596.

ABSTRACT A high-efficiency microwave power transmission (MPT) system based on an inverted class F (F^{-1}) rectifier for microwave wireless charging applications is presented in this paper. A left-hand circular polarization (LHCP) transmitting antenna (Tx) is designed based on a modified sequential phase rotation (SPR) divider integrated with a 2 × 2 array. The proposed Tx exhibits compact size with LHCP maximum gain of 11.85 dBi at 5.8 GHz. Furthermore, the receiver is composed of an LHCP receiving antenna (Rx) and a microwave F^{-1} rectifier. To realize the power radiated region of the Tx, an Rx with a wide beamwidth for minimizing distance loss is proposed, which has a 3-dB axial ratio (AR) beamwidth of 165.55° and 175.17° in the *x*-*z* and *y*-*z* planes, respectively. In addition, to improve the RF to DC conversion efficiency (η), the class F^{-1} harmonic processing network is utilized at the load of the rectifier that can process the voltage and current waveforms without using a DC pass filter. The proposed F^{-1} rectifier circuit occupies a compact area of 15.3 × 12.7 mm^2, and it exhibits an average η of 50% for the input power range from 4 to 20 dBm with a peak efficiency of 77.9% at 18 dBm. Overall, the experimental results show that our proposed system achieves a maximum power transmission efficiency (PTE) of 8.8% for wirelessly charging low-power multiple devices at a distance of 60-200 mm.

INDEX TERMS Circularly polarized antenna, harmonic processing, microwave rectifier, wireless power transmission (WPT), wireless charger.

I. INTRODUCTION

In recent years, advances in science and technology have enabled wireless power transmission (WPT) applications to be deployed in the industrial, scientific, and medical (ISM) fields such as smart-watch strap chargings [1], contactless battery chargers for cellular phones [2]–[4], and consumer electronics [5]. These aforementioned applications employ wireless charging technologies mainly based on inductive and resonant coupling, which requires two receiver and transmitter coils placed opposite to each other and/or spaced closely to transmit energy. As a result, these systems are capable of effectively charging only the device. Meanwhile, increasing device usage requires the WPT's power source to satisfy the need to charge many devices simultaneously. In addition to transmitting power over long distances [6]–[11], microwave power transmission (MPT) needs to transmit energy simultaneously to multiple devices whose receiving area is configurable through the antenna with high directivity.

In practice, the transmitter (Tx) and receiver (Rx) are misaligned over long distances, leading to polarization losses, which reduce the coupling efficiency. Therefore, several methods are used to solve the misalignment problem and increase the transmission efficiency of the WPT system, such as using a gain-boosting array technique [12], dual-layer printed circuit board (PCB) metamaterial [13], omnidirectional magnetic field based on cubic Tx [14], butterfly shape Tx [15], and multiple transmitters [16], [17]. Although these works achieved several good characteristics for improving the coupling efficiency, most of these structures are relatively complicated and sizeable. Hence, it is not suitable for MPT applications that aim to compact charging devices. For long

The associate editor coordinating the review of this manuscript and approving it for publication was Qi Luo.

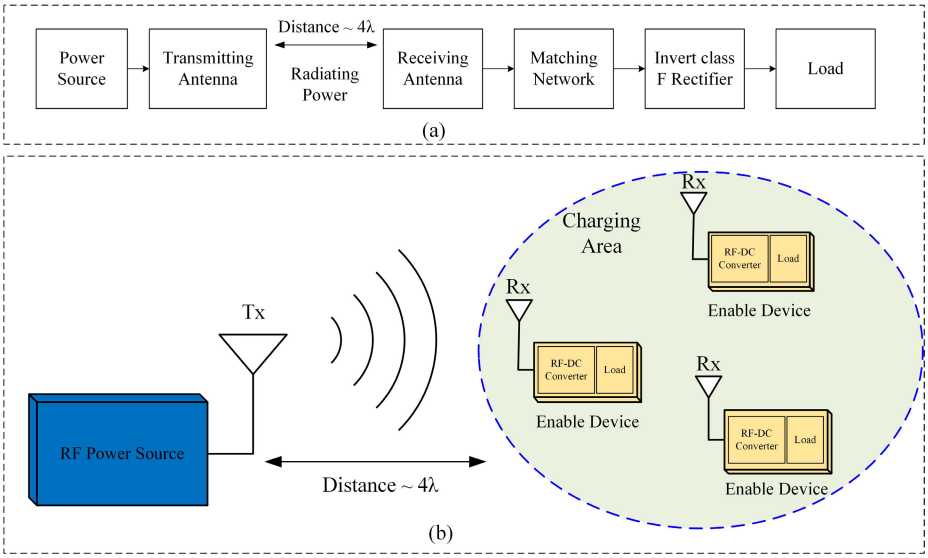

FIGURE 1. (a) Generalized block diagram of WPT system. (b) Proposed MPT system for charging multiple devices.

distances, circular polarization (CP) is the expected characteristic in antenna design, making system performance not be decreased by misalignment between Tx and Rx, and transmission energy is also preserved while moving. To realize low-profile antennas with high gain, several techniques have been developed recently, including slot antenna integrated waveguide (SIW) cavities [18]–[21], to further improve the structure gain by utilizing an antenna array with an SP feed [22], [23]. In [24], the copper ground plane with a 20 mm air gap was located under four microstrip square patches. Recently, for a compact structure, a patch antenna array feed composed of an SP network and 2 × 2 metasurfaces was presented in [25]. However, the drawback of these techniques is that the complex SP feeds are combined with multilayers creating air gaps between them, leading to challenges in fabrication and experimentation.

On the other hand, the rectenna model of the above WPT systems should feature: 1) flexible and ultra-lightweight structure, 2) multi-frequency bands, 3) wide dynamic range, and 4) high sensitivity with ultra-low input power [26]–[29]. Moreover, for the potential to be used in long-distance wireless charging of handheld devices at 5.8 GHz, the output DC power with high RF to DC conversion efficiency (η) and stable output DC voltage is needed in the rectifier design. For instance, a 5.8 GHz rectenna array was used in [30] to wirelessly power a small aircraft, where the DC output voltage can be converted from 18 dBm (63.1 mW) input power with η of 70% for an optimal load of 900 Ω.

In this paper, we propose and investigate a complete long-distance MPT system for charging multiple devices, as illustrated in Fig. 1. which consists of an SPR ring antenna and a class F^{-1} rectenna. A CP ring antenna is configured as the transmitter source, utilizing a high-directivity

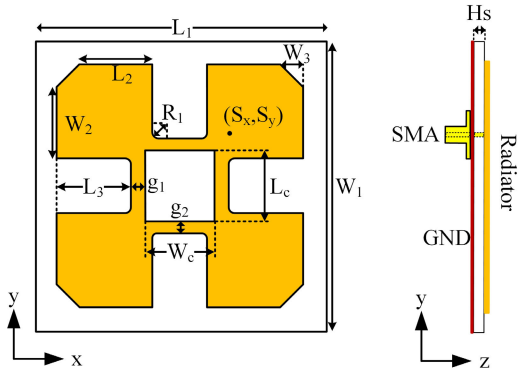

FIGURE 2. Radiator geometry of source antenna: (a) Top view, (b) Side view.

TABLE 1. Design parameters of the proposed transmitting source (unit: mm).

Parameter	W_1	L_1	W_2	L_2	W_3	L_3	W_c
Value	65	65	12.71	12.96	4.7	13.25	12.6
Parameter	L_c	S_x	S_y	R_1	g_1	g_2	H_s
Value	12.6	9	9	1	2.45	2.2	0.8

single-layer structure and easily integrated inside electronic devices. The receiver uses a rectenna consisting of a CP Rx antenna and a class F^{-1} rectifier, where Rx with a wide axial ratio (AR) beamwidth can receive stable power, minimizing misalignment. In addition, a class F^{-1} rectifier with high RF-DC conversion efficiency is proposed. The system battery charging capability, represented by the power transmission efficiency (PTE), has been tested in a laboratory environment, where power LEDs substitute sensor/IoT devices.

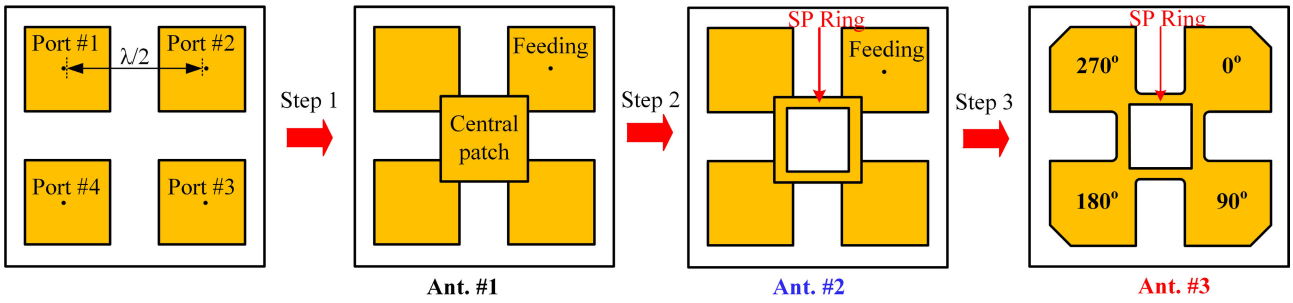

FIGURE 3. Detail design process of the proposed Tx antenna.

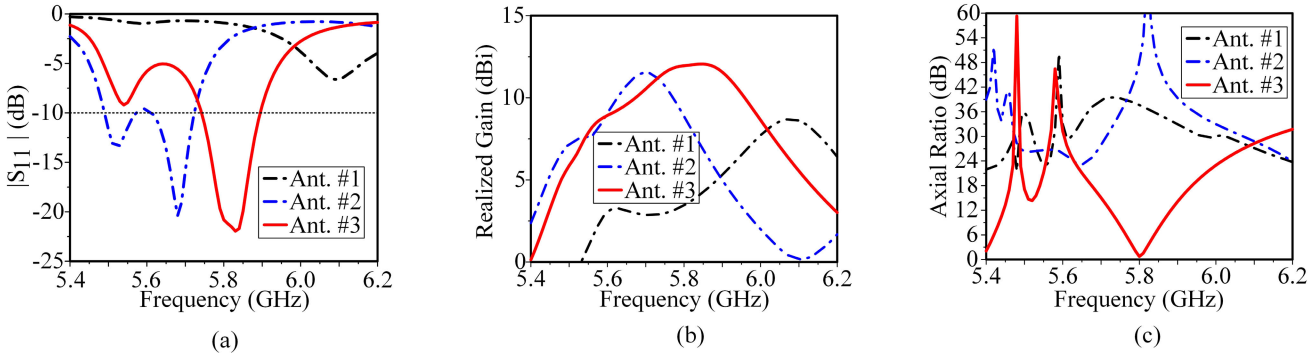

FIGURE 4. (a) simulated reflection coeffient (S_{11}) (b) Realized gain (c) Axial ratio (AR) for different prototype.

II. DESIGN OF MICROWAVE WIRELESS ENERGY TRANSMITTING ANTENNA

A. GEOMETRY OF THE ANTENNA

Fig. 2 shows the geometry of the proposed CP Tx source, which comprises a 2 × 2 array antenna cascaded around the central patch. A square-shaped cut patch at the center of the substrate yielded the SP ring. In addition, the length (Lc) and width (Wc) of the SP ring are slightly different to realize CP radiation. The Tx antenna is printed on Taconic TLY-5 substrate ($\varepsilon_r = 2.2$, $\tan\delta = 0.0009$, and thickness = 0.8 mm) with overall dimension of 65 × 65 × 0.8 mm^3.The proposed antenna is feed by a 50 Ω subminiature version-A (SMA) connector, the outer part of the SMA is connected to the ground plane, while the inner part passes through the ground plane and the substrate links to the patch at (Sx, Sy). The optimized parameters at 5.8 GHz are listed in Table 1.

B. DESIGN EVOLUTION

To clarify the design principle, the detailed development process and corresponding performance parameters of the proposed structure are shown in Fig. 3 and 4, respectively. Accordingly, to produce CP radiation with high directivity while requiring a compact and low-profile antenna, a square ring is cascaded with a 2 × 2 array to obtain a sequential phase rotation antenna and increase the antenna directivity. In contrast to previous sequential phase rotation structures [22]–[25], in this work, a square ring is used as a sequential phase power divider to make the structure more compact and straightforward. The SPR power divider is modified into microstrip lines with an approximately quarter-wavelength, connecting the patches to form a closed phase rotation for the input signal phase to easily rotate from the source patch to the other patch with steps of 0°, 90°, 180°, and 270°.

To describe the antenna design process in detail, different design steps and equivalent performances are shown in Fig. 3. Initially, the chosen structure consists of a conventional 2 × 2 array with elements spaced approximately $\lambda_0/2$ (λ_0 is the wavelength referring to the center frequency of 5.8 GHz). However, an array antenna shows that the array needs to be excited by four ports simultaneously or combined with an even power divider. In step 1, a patch was added at the center to create an Ant. 1, where the structure uses only single layers and is excited by a single port. The second structure (Ant. 2) is adapted by Ant. 1 and the center cut patch creates a square loop. Ant. 3 is the complete proposed structure based on Ant. 2, and the outer corner with a quarter-arc improved the CP radiation efficiency. For a convenient comparison, the parameters in all configurations are listed in Table 1.

The corresponding reflection coefficients for the three configurations are shown in Fig. 4(a). In Ant. 1, owing to the structure composed of conventional patch antennas, it achieves poor impedance matching and a peak gain of 8.7 dBi at 6.1 GHz, as shown in Fig. 4(b). Based on

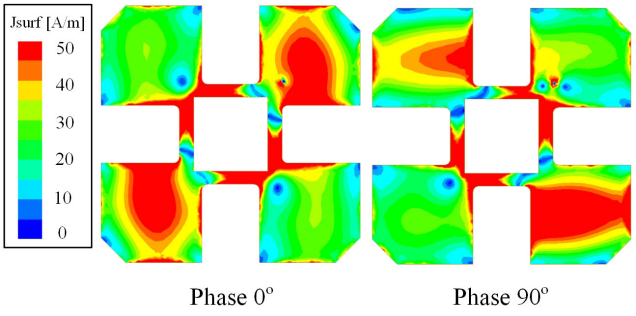

FIGURE 5. Current distribution of the transmitting antenna for different phase angles.

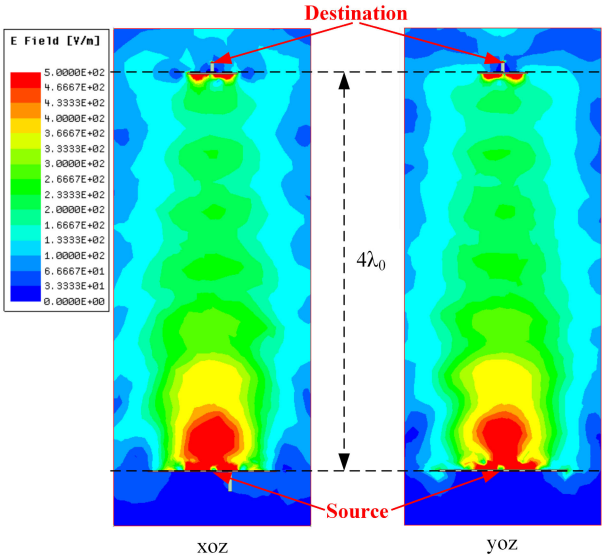

FIGURE 6. Coupling electric field when the transmission source is excited.

the sequential phase rotation principle described in previous studies [22]–[25], a square slot is added to the center of Ant. 1. Ant. 2 structure shows good impedance matching at low frequencies with two resonances. In addition, the gain value improve at about 11.5 dBi at 5.7 GHz. This is because the additional square slot creates an SPR ring, where the current distribution becomes more concentrated at the arm of the antenna, thereby improving the radiation efficiency. Fig. 4(c) shows that both Ant. 1 and Ant. 2 reaches CP radiation. In this case, outer corners are inserted to make the AR value at 5.8 GHz nearly 0 dB. In addition, a 2 × 2 patch array cascade with a square ring center, where poor coupling between the patch and square ring is a cause of not achieving high radiation. Therefore, to increase the coupling between the patches and the square ring, quarters of the radius R_1 circle are added, assisting to reinforce the cascade between them while achieving a maximum gain, i.e., 11.98 dBi at 5.8 GHz. In addition, to further clarify the phenomenon of generating CP, we have examined how the current distribution on the metal surface at 5.8 GHz, as shown in Fig. 5. It is shown that the phase distribution between two opposite arms of the antenna is always 180° in the vertical and horizontal directions, which agrees with the equivalent model Ant. 3 in Fig. 3.

To transmit energy effectively over a long distance with a high directivity antenna, the field distribution should have radiation similar to a plane wave. Here, the radiative focusing of the electric field at the receiver is obtained, as shown in Fig. 6. This indicates that the energy emitted at the Tx antenna is completely concentrated towards the receiver, where the air gap between the two investigated points is approximately $4\lambda_0$. The energy-concentration characteristic satisfies the wireless energy transmission requirements with high efficiency for targets at long distances.

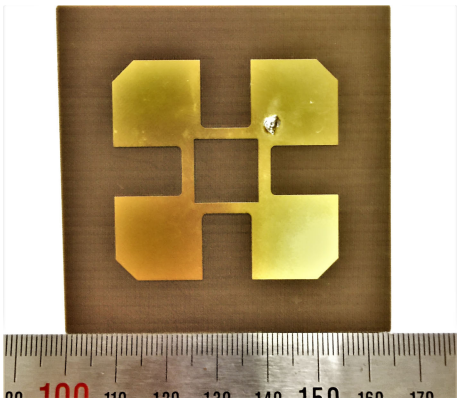

FIGURE 7. Prototype of the proposed Tx antenna.

C. SIMULATED AND MEASURED RESULTS

The fabricated prototype of the proposed CP Tx source is shown in Fig. 7. The experimental results of the reflection coefficient S_{11} were verified using a vector network analyzer (Agilent 8719D). As shown in Fig. 8(a), the results indicate good agreement between simulation and measurement over a bandwidth of 5.74 - 5.87 GHz (1.72%). The measured results are presented in Fig. 8(b), where the peak gain of the transmitting antenna reaches a maximum of 11.85 dBi at 5.8 GHz and more than 11.4 dBi while the simulation peak gain is 11.98 dBi and more than 11.7 dBi over the entire bandwidth. In addition, Fig. 8(b) shows that the simulated and measured values of the < 3 dB axial ratio (AR) bandwidth is 5.78 - 5.81 GHz, and the AR value is close to 0 dB at the center frequency. The radiation patterns of the proposed prototype at the center frequency in the *x*-*z* and *y*-*z* planes are illustrated in Fig. 9. In this case, the simulation results show that the LHCP gain value must be greater than 20 dB of cross-polarized RHCP in both the *x*-*z* and *y*-*z* planes. Nevertheless, a radiation pattern is measured in the *y*-*z* plane that satisfies this condition, while the value is greater than 16 dB in the *x*-*z* plane. The difference between the two radiation patterns is the cause of the measurement. In measurement, the process of measuring the radiation pattern at the two *x*-*z* and *y*-*z* planes are two different steps. The position of the antenna needs to be adjusted to 0 degrees and 90 degrees to the *x*-*z* and *y*-*z* planes, respectively. Therefore, it is challenging to avoid misaligning the antenna's position while rotating,

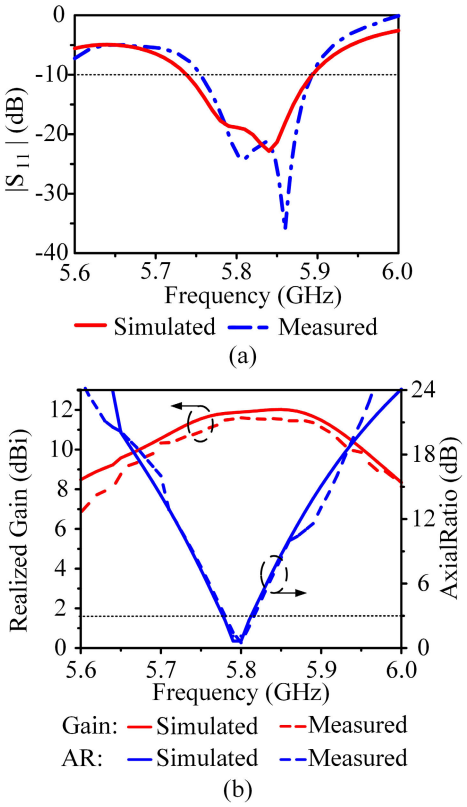

FIGURE 8. Simulated and measured (a) $|S_{11}|$, and (b) AR and realized gain values.

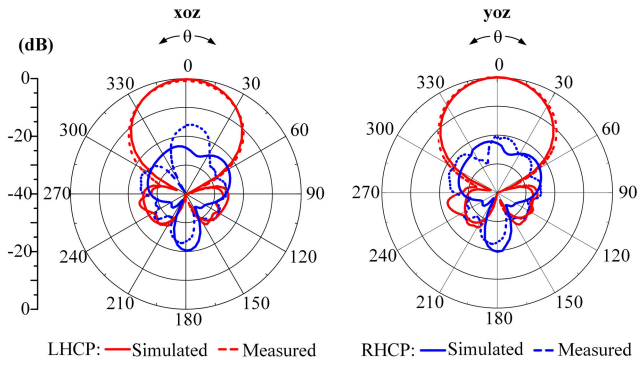

FIGURE 9. Simulated and measured radiation patterns in *x-z* and *y-z* planes.

leading to inconsistency with the axial ratio. Since the proposed antenna is symmetrical, the radiation patterns at the *y-z* and *x-z* planes are equivalent. In addition, the antenna realizes a high-gain LHCP radiation in the broadside direction with a sidelobe level (SLL) of less than −20.3 dB. The half-power beamwidths (HPBW) were 44.57° and 45° in the *x-z* and *y-z* planes, respectively.

The performance of the proposed antenna is compared with that of recent high-gain antennas, as summarized in Table 2. It is observed that the proposed antenna integrated with SP feed exhibits a smaller dimension and higher directivity while using a single layer similar to the prior designs [18],[21],[23].

TABLE 2. Comparision with lastest relevant works.

Reference	Method	Electrical size (λ_0 x λ_0)	No. of PCB layers	Peak gain (dBi)
[18]	Slot, SIW	0.69 x 0.64	1	7.6
[21]	SIW	1.31 x 1.31	1	10.4
[23]	SPR	1.5 x 1.5	1	11.5
[24]	SPR	1.32 x 1.32	2	13.2
[25]	SPR, meta	1.26 x 1.26	2	12.08
This work	**SPR**	**1.26 x 1.26**	**1**	**11.85**

λ_0: Air wavelength SPR: Sequential phase rotation

SIW: Substrate integrated waveguide

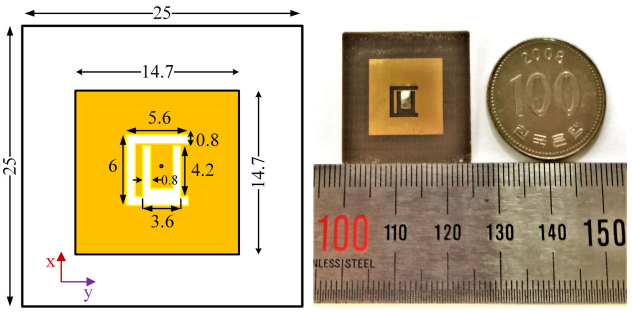

FIGURE 10. Structure of the proposed receiving antenna: (a) simulated and (b)Fabricated.

Although the SP feed structures in [24], [25] provide a higher gain, the design is more complicated when a feeding network and more dielectric layers are required.

III. RECTENNA

A. RECEIVING ANTENNA DESIGN

Various configurations have been investigated for selecting suitable receiver antennas. Here, the patch antenna incorporates the slot structure to achieve circular polarization and a wide beamwidth. The optimized design parameters and top view of the proposed Rx antenna are shown in Fig. 10. Two U-shaped slots were etched orthogonally at the center of the patch to generate circular polarization. The receiving antenna was printed on both sides of the Taconic TLY-5 material (ϵ_r = 2.2, thickness = 0.8 mm). Based on the center frequency, the geometric parameters were approximated to obtain the desired resonant mode in the proposed structure. Here, the size of the central patch is slightly larger than $\lambda_0/4$, whereas the size of the ground plane is approximately $\lambda_0/2$. The size of the ground plane is selected such that it can be easily integrated with wearable devices. In practice, the antenna is excited at the center of the patch with a 50 Ω coaxial cable. The outer part of the coaxial cable was connected to the ground plane, while the inner part passed through the ground plane and substrate to connect to the radiator. The design optimization is carried out via the series ANSYS Electronics Desktop simulation targeting the circular

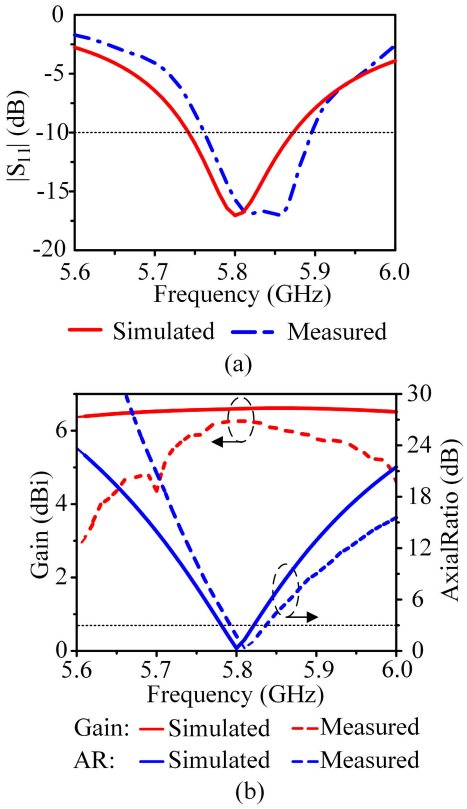

FIGURE 11. Simulated and measured (a) $|S_{11}|$, and (b) AR and realized gain values.

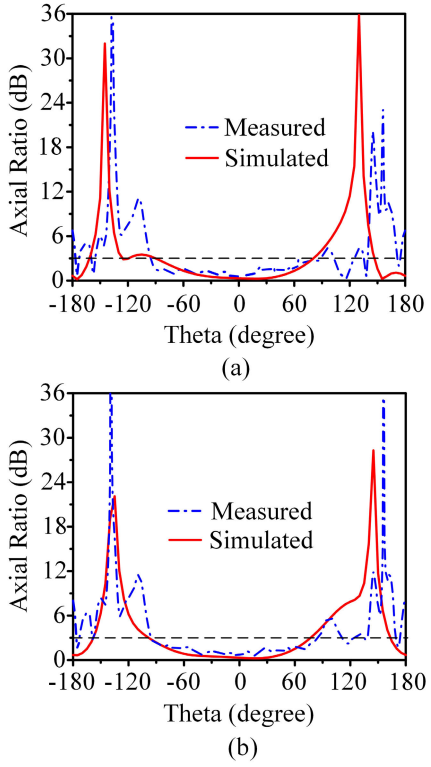

FIGURE 12. Simulated and measured AR: (a) *x-z* plane and, (b) *y-z* plane.

polarization and wide-HPBW at 5.8 GHz. Fig 11 shows a comparison of the simulated and measured results for the

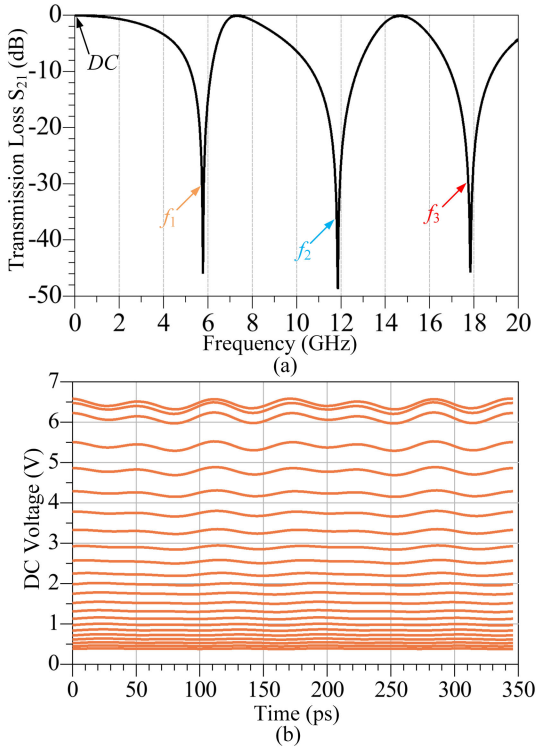

FIGURE 13. (a) Frequencies response of rectifier using F^{-1} harmonic processing network where f_1 is fundamental frequency; f_2, f_3 are second and third harmonics. (b) Output DC voltage of proposed rectifier at time domain.

proposed CP Rx antenna. The results indicate that the measured resonance mode shifts slightly up to a higher frequency. The frequency shift was negligible because of the fabrication error, and the measured results were still within the acceptable range. The S_{11} measured results agree well with the simulated ones within a bandwidth of 5.77-5.89 GHz, as observed in Fig. 11(a). A comparison between the simulated and measured results for the peak gain and AR values is shown in Fig 11(b). This indicates that the measured gain has a maximum of 6.25 dBi at 5.62 GHz, whereas the simulated one is 6.8 dBi. The measured and simulated AR values were nearly zero at the central frequency. The measured 2D radiation pattern is an experiment in an anechoic chamber with scan angles given in Fig. 12. The radiation of the proposed Rx is also LHCP radiation to match the incoming source. At the central frequency, the proposed Rx achieves wide-AR beamwidths of 172.6° and 161.3° in the *x-z* and *y-z* planes, respectively.

B. F^{-1} RECTIFIER DESIGN

Charge pump rectifiers have received attention as a key part of receiving rectenna to power electric-consuming devices in MPT systems. The RF to DC power conversion efficiency (PCE) is the main factor of the rectifier used to evaluate system performance. Several techniques are currently applied to rectifier circuits to increase their efficiency and power response from a few milliwatts to hundreds of milliwatts at

TABLE 3. Comparison with Previous Work.

Ref.	Year	Frequency (GHz)	Peak PCE (%)	Dynamic range (dBm) for PCE > 50%
[31]	2014	5.8	80	7 to 18.75
[32]	2017	5.8	78	10 to 16.02
[33]	2018	2.45	63	8.5 to 32.5
[34]	2019	2.45	80.4	1 to 16.5
[35]	2020	2.6	82	-7.5 to 10
This work	**2021**	**5.8**	**77.9**	**5 to 21**

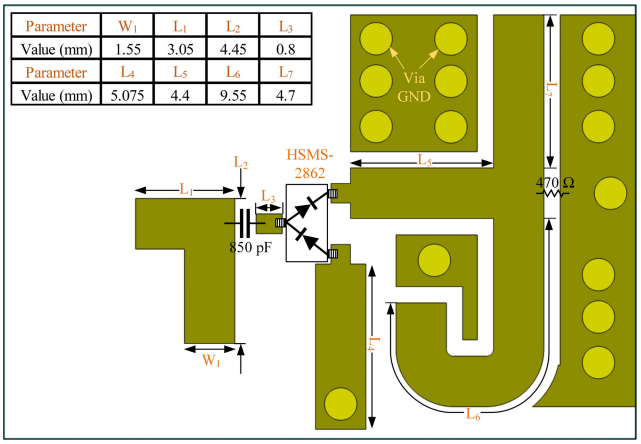

FIGURE 14. Layout of the proposed rectifier.

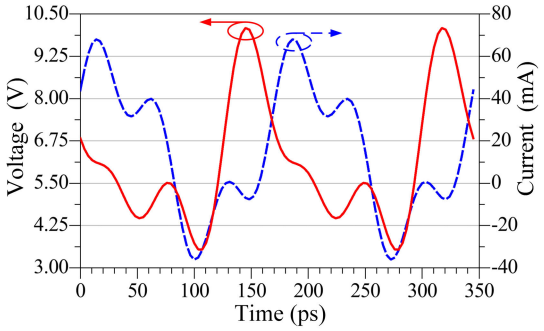

FIGURE 15. Voltage and current waveforms at the output of Schottky diode.

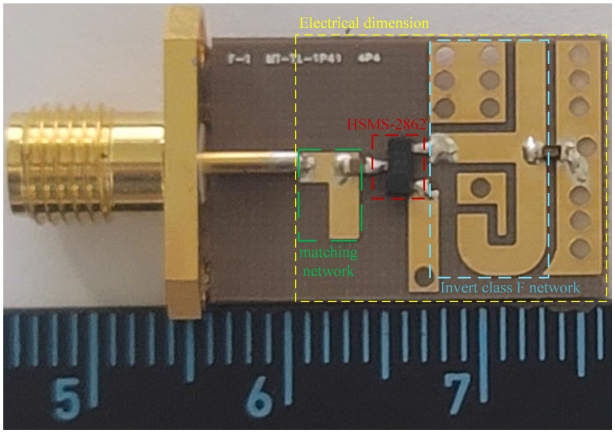

FIGURE 16. Photograph of the proposed rectifier.

microwave frequencies, as indicated in Table 3. For instance, based on a theoretical analysis of the RF-DC conversion efficiency for a class F at load [31], a 5.8 GHz rectifier's PCE is enhanced up to 80% at 60 mW, and to reduce the weight of a satellite in an internal wireless system for satellites [32], a class F charge-charge pump rectifier is designed to convert 30 mW receiving RF signal to DC voltage with efficiency of 78%. By utilizing the power recycling technique [33], a 2.45 GHz rectifier can achieve a PCE of 63% at 316.23 mW. Using an F^{-1} harmonic termination network, the rectifier in [34] has a peak RF-DC conversion efficiency of 80.4% at an input power of 20 mW. In [35], a harmonic-recycling method was used in a 2.6 GHz rectifier to increase its PCE up to 18% compared with the conventional design using a DC pass filter or harmonic suppression network at 5 dBm (3.16 mW). However, because of the complex rectifier topology, these previous works did not achieve a compact size to integrate with these small receiving antennas. In particular, for the charge-pump class F load, which functions with a quarter wavelength of a fundamental frequency. Thus, based on the harmonic processing concept, we proposed the F^{-1} rectifier, which obtains both compact size and acceptable PCE at an RF input power at 5.8 GHz.

In contrast to class F^{-1} harmonic processing techniques in power amplifiers [36], the F^{-1} rectifier processes both the fundamental frequency and its harmonic frequencies to convert an RF signal at the output of Schottky diodes into DC voltage without using a shunt capacitor, as shown in Fig. 13. However, the output DC voltage of our proposed rectifier is not smooth because of the lack of a shunt capacitor, and this is the only disadvantage of our proposed design, which can be traded-off to obtain other benefits as follows: (1) there is no dissipated power on the parasitic resistance of the shunt capacitor; (2) the power dissipation on the RS resistance of the Schottky diode is greatly reduced from the orthogonal effect between the voltage and current waveforms of the class F^{-1} harmonic processing network; (3) the PCE is increased at the maximum RF input power of the rectifier, which is the same as a characteristic of the class F^{-1} harmonic terminal network in the power amplifier design. Fig. 14 shows the layout of the proposed rectifier, in which W_1 is the electrical width of the transmission lines with a characteristic impedance of 50 Ω, L_1 and L_2 are used for the input matching network, while the forward bias applied voltage of the Schottky diode is dependent on the electrical length of L_4. L_5 is a resonant transmission line at the second harmonic frequency, and L_6 and L_7 are open transmission lines at the fundamental and second harmonic frequencies. Thus, their impedance is related to wavelengths as follows.

$$\begin{cases} L_6 \approx \dfrac{\lambda_1}{4} \Rightarrow \begin{cases} Z_1 \approx 0.36 + 53j \\ Z_3 \approx 1 - 52j \end{cases} \\ L_5 \& L_7 \approx \dfrac{\lambda_2}{4} \Rightarrow Z_2 \approx \infty \end{cases} \quad (1)$$

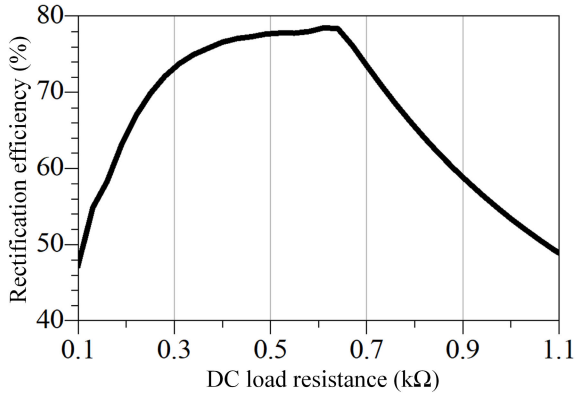

FIGURE 17. The optimal load resistance analyzing.

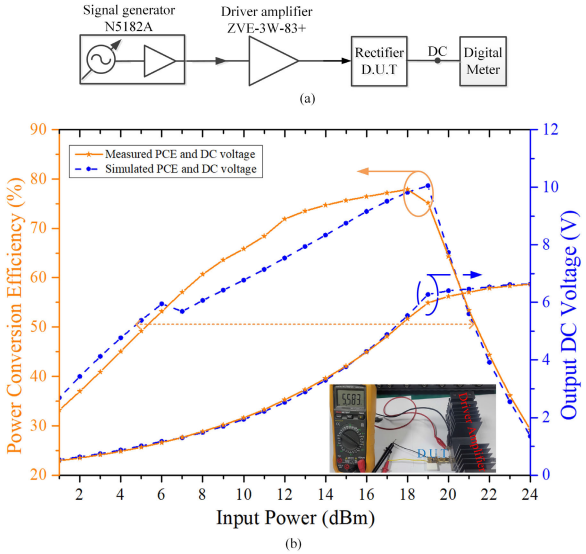

FIGURE 18. (a) Measurement setup for proposed rectifier as device under test, and (b) Measured results compared with simulated results.

Here, λ_1 and λ_2 are the wavelengths of the fundamental and second harmonic frequencies, respectively. Z_1 is the impedance at the operating frequency, and Z_2 and Z_3 are the harmonic impedances at the second and third orders, respectively. By controlling the impedance of the operating frequency and its harmonics, the voltage and current waveforms at the output of the Schottky diode are shown in Fig. 15, where the orthogonality between them can be seen at the time when the peak reverse current overlaps with the minimum voltage; hence, the dissipated power $P_{dis.}$ on Schottky diode's resistance R_S is expressed as:

$$P_{dis.} = \frac{1}{T_R}\int_{T_R}^{\circ} V_R I_R d\theta \tag{2}$$

Here, T_R is the period of the reverse current I_R, and V_R is the voltage applied at cathode of Schottky diode.

The electrical dimensions of the proposed rectifier are 16×12 mm^2 and fabricated on a TLY-5 substrate with a dielectric constant ε_r of 2.2 and thickness of 0.5 mm as shown in Fig. 16. Considering in Fig. 17 is the optimal resistance analysis, which can be determined from the relationship between DC load resistance and the rectification efficiency. Thus the optimal resistance value is 650 Ω for RF-DC conversion efficiency of 78.4%. The measurement setup and measured results of the proposed rectifier are shown in Fig. 18; since the proposed rectifier's maximum input power is over 20 dBm (100 mW), the driver amplifier is applied to supply a stable single tone RF power from 1 to 24 dBm at the input of rectifier. The measured PCE was 75.16% and 3.5% less than the simulated results at 19 dBm. Although the measured PCE is higher than its simulated result when input power from 7 to 18 dBm, the dynamic measurement range is 0.5 dB narrower than its simulation one. This error could stem from the low optimal load resistance, which is 470 Ω, and causes a large gap between the measured and simulated DC powers.

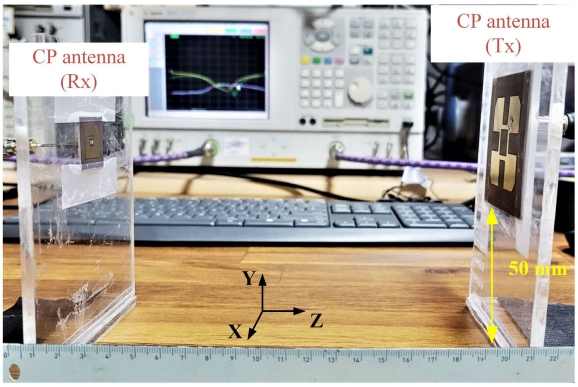

FIGURE 19. Measurement setup for transmission coefficient S_{21} at 200 mm.

IV. MICROWAVE EXPERIMENT AND EVALUATION

Initially, each circularly polarized component of the MPT system (Tx, Rx, and rectifier) was investigated separately and verified experimentally.

At long distances, the relationship between the Tx gain and beamwidth is illustrated by

$$G_t = \frac{Area\ of\ Sphere}{Area\ of\ Antenna\ Pattern} \tag{3}$$

$$= (4\pi r^2)\cdot\frac{1}{\pi r^2 sin(\theta/2)sin(\phi/2)} \tag{4}$$

$$= \frac{4}{sin(\theta/2)sin(\phi/2)}, \tag{5}$$

where G_t is the gain of the transmitting antenna, r is radius of the isotropic sphere, and θ and ϕ are the azimuth and elevation beamwidth in radians, respectively. In this case, because the structure is symmetrical, the azimuth and elevation beamwidths are similar. Based on the beamwidth and desired distance d, the charge area was calculated using (6):

$$S = \pi(d\tan(2\arcsin(\frac{2}{\sqrt{G_t}})))^2. \tag{6}$$

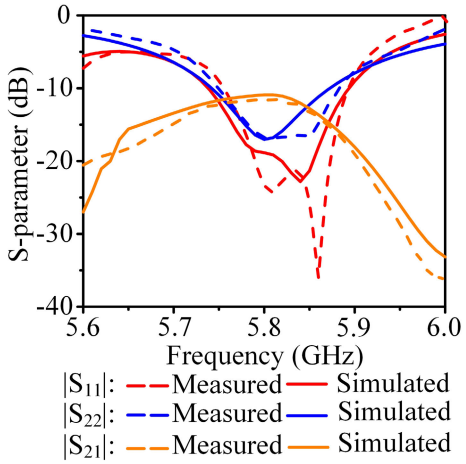

FIGURE 20. Simulated and measured S-parameters of the propsoed MPT link.

Moreover, the MPT link efficiency can be computed using the following equation [9]:

$$P_r = \frac{G_t G_r \lambda_0^2}{(4\pi d)^2}(1 - |S_{11}|^2)(1 - |S_{22}|^2)e_p P_t \approx |S_{21}|^2 P_t. \quad (7)$$

In (7), the received power is widely used to calculate the maximum possible power in a radio system, where many factors reduce the received energy.

For further verification, Fig. 19 shows a photograph of the S-parameter measurement setup of the MPT link. The transmitting and receiving antennas are connected to a vector network analyzer (8719D), and the Rx position was verified inside the energy area (6). Both antennas were mounted on an acrylic material holder, which kept the antenna at a height of 50 mm away from the ground to avoid unwanted ground reflections. In addition, to determine the stable operation of the links between the two antennas, several cases were verified for the different locations and angles of the receiving antenna. First, both antennas' reflection coefficients are measured under fixed conditions (range and angle), as shown in Fig. 20, and this indicates that the transmitting and receiving antennas radiate more than 98% of the energy. Therefore, the reflection coefficient in Eq. (7) was ignored. Furthermore, the MPT link uses circular polarization, so the polarization mismatch is almost zero. In this study, the microwave power link is simulated using the ANSYS high-frequency structure simulator (HFSS), which can consider the simulation environments to cover all influencing factors. In this case, the simulated value of S_{21} represents the power transfer capability of the MPT link, as mentioned in (7). Second, we measured the transmission loss of our MPT system when the distance between Rx and Tx increases from 60 mm to 200 mm, as shown in Fig. 21(a). For angle conditions, the transmission coefficient ($|S_{21}|$) between the Tx and Rx antennas was measured when Rx was at angle of 0°, 15°, 45°, and 60° in the *y*-*z* plane, respectively, as shown in Fig. 21(b). Finally, to verify the advantage of the circular polarization in reducing the polarization loss, the antenna link distance was fixed at

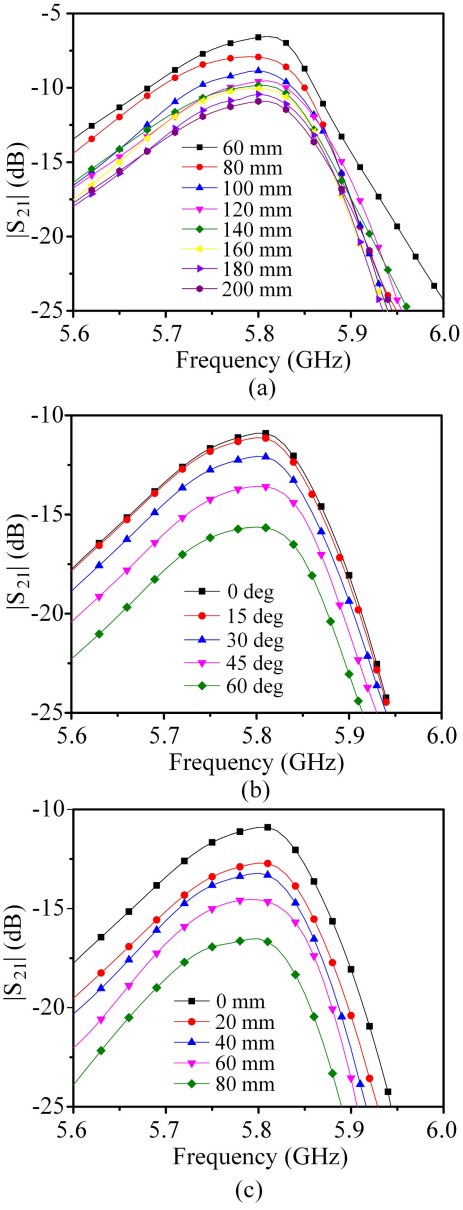

FIGURE 21. Measured $|S_{21}|$ values: (a) with moving distance Rx in oz direction. Fixed MPT link distance at 200mm (b) angle misalignment (c) shift Rx in ox direction.

200 mm, and the Rx antenna was misaligned with Tx from 0 to 80 mm in the *ox* direction, as illustrated in Fig. 21(c). This indicates a 5-dB loss in the measured S_{21} for all cases, where the MPT link efficiency reached 9% at a distance of 200 mm. In summary, the transmission characteristics of the proposed system were relatively stable at different locations of the Tx and Rx antennas.

The rectifier is integrated with the backside of the receiving antenna, referred to as a rectenna, as shown in Fig. 22. Here, we use four rectennas with the rectifiers rotated in 90°,and three of them are used to demonstrate the circular polarization of the receiving antenna and the radiated energy region of the source. The remaining one was used to measure the output

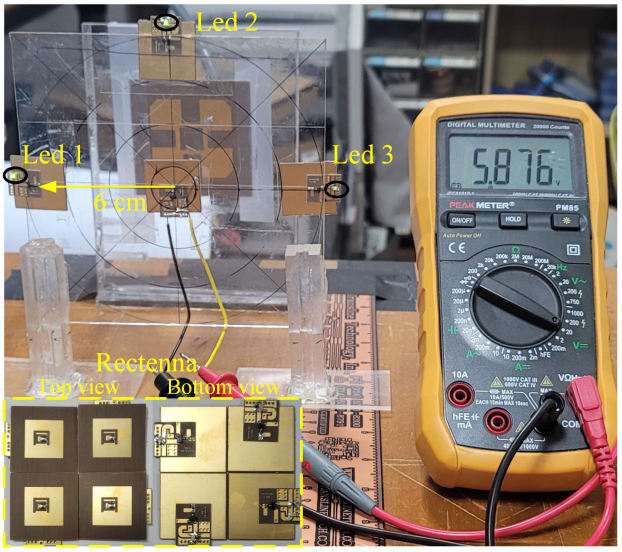

FIGURE 22. Measurement setup for microwave power transfer system.

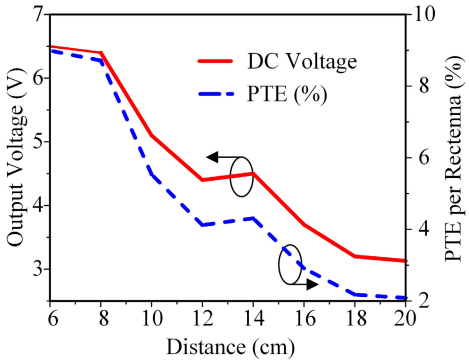

FIGURE 23. Measured results of the proposed MPT system.

voltage at different distances. In addition, the measurement setup for the MPT system was implemented, where the proposed rectenna was kept in the light of sight direction with the source at a distance of 100 mm. The transmitter source radiates 30 dBm (1 W) power based on FCC rules for the maximum transmit output power in the ISM band. While measuring system performance, the output port of the middle rectenna is connected to a digital multimeter (DMM) to display the converted DC voltage. The measured results show that the rectenna can yield an output voltage of 5.876 V at a distance of 100 mm. Furthermore, to determine the charging area, as calculated in (6), the LEDs are appended to three rectenna arranged around in a circle. The results show that the LEDs turned on within a radius of 60 mm. The measured DC output voltage and total PTE are functions of the distance with the 470 Ω load resistor, as shown in Fig. 23. After collecting the data shown in Fig. 21, the overall system efficiency changes from 2.2% to 8.8% as the receiving distance varies in the range of 60-200 mm.

The proposed MPT system presents a technology that provides many opportunities for several practical applications. The proposed design can charge various low-power devices such as LED displays and sensors for static wireless charging applications, where these devices are placed directly with the charger. For moving applications, the proposed scalable WPT system is suitable for charging smartwatch wearable devices when they move and recharge in a fixed energy region without removing them from the body.

V. CONCLUSION

This paper proposes an efficient microwave WPT system for charging multiple devices at long distances by employing a compact CP Tx antenna with high directivity and a high conversion efficiency F^{-1} rectifier at 5.8 GHz. Theoretical analysis shows that the proposed Tx can achieve a high concentration of energy toward the Rx antenna. Furthermore, the rectifier is connected behind the wide-beamwidth Rx antenna to achieve a simple, compact rectenna for harvesting EM waves and reducing misalignment losses. The overall system was verified with distances varying from 60 to 200 mm. The achievable maximum PTE efficiency was 8.8%, and the energy was received within an area with a radius of 60 mm. In general, the proposed system is suitable for the simultaneous powering of many low-power devices.

REFERENCES

[1] S. Jeong, D.-H. Kim, J. Song, H. Kim, S. Lee, C. Song, J. Lee, J. Song, and J. Kim, "Smartwatch strap wireless power transfer system with flexible PCB coil and shielding material," *IEEE Trans. Ind. Electron.*, vol. 66, no. 5, pp. 4054–4064, May 2019.

[2] P. D. H. Re, S. K. Podilchak, S. A. Rotenberg, G. Goussetis, and J. Lee, "Circularly polarized retrodirective antenna array for wireless power transmission," *IEEE Trans. Antennas Propag.*, vol. 68, no. 4, pp. 2743–2752, Apr. 2020.

[3] C.-G. Kim, D.-H. Seo, J.-S. You, J.-H. Park, and B. H. Cho, "Design of a contactless battery charger for cellular phone," *IEEE Trans. Ind. Electron.*, vol. 48, no. 6, pp. 1238–1247, Dec. 2001.

[4] C. Xu, Y. Zhuang, C. Song, Y. Huang, and J. Zhou, "Dynamic wireless power transfer system with an extensible charging area suitable for moving objects," *IEEE Trans. Microw. Theory Techn.*, vol. 69, no. 3, pp. 1896–1905, Mar. 2021.

[5] H. Hoang, S. Lee, Y. Kim, Y. Choi, and F. Bien, "An adaptive technique to improve wireless power transfer for consumer electronics," *IEEE Trans. Consum. Electron.*, vol. 58, no. 2, pp. 327–332, May 2012.

[6] C. Liu, Y.-X. Guo, H. Sun, and S. Xiao, "Design and safety considerations of an implantable rectenna for far-field wireless power transfer," *IEEE Trans. Antennas Propag.*, vol. 62, no. 11, pp. 5798–5806, Nov. 2014.

[7] N. Shinohara, "History and innovation of wireless power transfer via microwaves," *IEEE J. Microw.*, vol. 1, no. 1, pp. 218–228, Jan. 2021.

[8] M. Xia and S. Aissa, "On the efficiency of far-field wireless power transfer," *IEEE Trans. Signal Process.*, vol. 63, no. 11, pp. 2835–2847, Jun. 2015.

[9] C. Liu, Y. Zhang, and X. Liu, "Circularly polarized implantable antenna for 915 MHz ISM-band far-field wireless power transmission," *IEEE Antennas Wireless Propag. Lett.*, vol. 17, no. 3, pp. 373–376, Mar. 2018.

[10] D. Belo, D. C. Ribeiro, P. Pinho, and N. B. Carvalho, "A selective, tracking, and power adaptive far-field wireless power transfer system," *IEEE Trans. Microw. Theory Techn.*, vol. 67, no. 9, pp. 3856–3866, Sep. 2019.

[11] A. Dwivedi, P. Rajbhar, and N. Tiwari, "Long distance power transfer technique: A review," *J. Mechtron. Robot.*, vol. 3, no. 1, pp. 208–214, Jan. 2019, doi: 10.3844/jmrsp.2019.208.214.

[12] B. Zhao, N.-C. Kuo, and A. M. Niknejad, "A gain boosting array technique for weakly-coupled wireless power transfer," *IEEE Trans. Power Electron.*, vol. 32, no. 9, pp. 7130–7139, Sep. 2017.

[13] Y. Cho, J. J. Kim, D.-H. Kim, S. Lee, H. Kim, C. Song, S. Kong, H. Kim, C. Seo, S. Ahn, and J. Kim, "Thin PCB-type metamaterials for improved efficiency and reduced EMF leakage in wireless power transfer systems," *IEEE Trans. Microw. Theory Techn.*, vol. 64, no. 2, pp. 353–364, Feb. 2016.
[14] N. Ha-Van and C. Seo, "Analytical and experimental investigations of omnidirectional wireless power transfer using a cubic transmitter," *IEEE Trans. Ind. Electron.*, vol. 65, no. 2, pp. 1358–1366, Feb. 2018.
[15] N. Ha-Van and C. Seo, "Modeling and experimental validation of a butterfly-shaped wireless power transfer in biomedical implants," *IEEE Access*, vol. 7, pp. 107225–107233, 2019.
[16] R. Johari, J. V. Krogmeier, and D. J. Love, "Analysis and practical considerations in implementing multiple transmitters for wireless power transfer via coupled magnetic resonance," *IEEE Trans. Ind. Electron.*, vol. 61, no. 4, pp. 1774–1783, Apr. 2014.
[17] T. Arakawa, S. Goguri, J. V. Krogmeier, A. Kruger, D. J. Love, R. Mudumbai, and M. A. Swabey, "Optimizing wireless power transfer from multiple transmit coils," *IEEE Access*, vol. 6, pp. 23828–23838, 2018.
[18] Y. Xu, Z. Wang, and Y. Dong, "Circularly polarized slot antennas with dual-mode elliptic cavity," *IEEE Antennas Wireless Propag. Lett.*, vol. 19, no. 4, pp. 715–719, Apr. 2020.
[19] D. Yang, F. Cao, and J. Pan, "A single-layer dual-frequency shared-aperture SIW slot antenna array with a small frequency ratio," *IEEE Antennas Wireless Propag. Lett.*, vol. 17, no. 6, pp. 1048–1051, Jun. 2018.
[20] T. Liang, Z. Wang, and Y. Dong, "A circularly polarized SIW slot antenna based on high-order dual-mode cavity," *IEEE Antennas Wireless Propag. Lett.*, vol. 19, no. 3, pp. 388–392, Mar. 2020.
[21] T. Yang, Z. Zhao, D. Yang, and Z. Nie, "A single-layer circularly polarized antenna with improved gain based on quarter-mode substrate integrated waveguide cavities array," *IEEE Antennas Wireless Propag. Lett.*, vol. 19, no. 12, pp. 2388–2392, Dec. 2020.
[22] S.-K. Lin and Y.-C. Lin, "A compact sequential-phase feed using uniform transmission lines for circularly polarized sequential-rotation arrays," *IEEE Trans. Antennas Propag.*, vol. 59, no. 7, pp. 2721–2724, Jul. 2011.
[23] W. Yang, J. Zhou, Z. Yu, and L. Li, "Bandwidth- and gain-enhanced circularly polarized antenna array using sequential phase feed," *IEEE Antennas Wireless Propag. Lett.*, vol. 13, pp. 1215–1218, 2014.
[24] W. Hu, D. Inserra, G. Wen, and Z. Chen, "Wideband low axial ratio and high-gain sequentially rotated antenna array," *IEEE Antennas Wireless Propag. Lett.*, vol. 17, no. 12, pp. 2264–2268, Dec. 2018.
[25] S. X. Ta and I. Park, "Compact wideband circularly polarized patch antenna array using metasurface," *IEEE Antennas Wireless Propag. Lett.*, vol. 16, pp. 1932–1936, 2017.
[26] V. Palazzi, J. Hester, J. Bito, F. Alimenti, C. Kalialakis, A. Collado, P. Mezzanotte, A. Georgiadis, L. Roselli, and M. M. Tentzeris, "A novel ultra-lightweight multiband rectenna on paper for RF energy harvesting in the next generation LTE bands," *IEEE Trans. Microw. Theory Techn.*, vol. 66, no. 1, pp. 366–379, Jan. 2018.
[27] C. Song, Y. Huang, P. Carter, J. Zhou, S. Yuan, Q. Xu, and M. Kod, "A novel six-band dual CP rectenna using improved impedance matching technique for ambient RF energy harvesting," *IEEE Trans. Antennas Propag.*, vol. 64, no. 7, pp. 3160–3171, Jul. 2016.
[28] P. Lu, X.-S. Yang, J.-L. Li, and B.-Z. Wang, "A compact frequency reconfigurable rectenna for 5.2- and 5.8-GHz wireless power transmission," *IEEE Trans. Power Electron.*, vol. 30, no. 11, pp. 6006–6010, Nov. 2015.
[29] S. Haddadian and J. C. Scheytt, "Analysis, design and implementation of a fully integrated analog front-end for microwave RFIDs at 5.8 GHz to be used with compact MIMO readers," *IEEE J. Radio Freq. Identificat.*, vol. 4, no. 4, pp. 476–490, Dec. 2020.
[30] Y. Yang, J. Li, L. Li, Y. Liu, B. Zhang, H. Zhu, and K. Huang, "A 5.8 GHz circularly polarized rectenna with harmonic suppression and rectenna array for wireless power transfer," *IEEE Antennas Wireless Propag. Lett.*, vol. 17, no. 7, pp. 1276–1280, Jul. 2018.
[31] J. Guo, H. Zhang, and X. Zhu, "Theoretical analysis of RF-DC conversion efficiency for class-F rectifiers," *IEEE Trans. Microw. Theory Techn.*, vol. 62, no. 4, pp. 977–985, Apr. 2014.
[32] C. Wang, N. Shinohara, and T. Mitani, "Study on 5.8-GHz single-stage charge pump rectifier for internal wireless system of satellite," *IEEE Trans. Microw. Theory Techn.*, vol. 65, no. 4, pp. 1058–1065, Apr. 2017.
[33] Y. Y. Xiao, Z.-X. Du, and X. Y. Zhang, "High-efficiency rectifier with wide input power range based on power recycling," *IEEE Trans. Circuits Syst. II, Exp. Briefs*, vol. 65, no. 6, pp. 744–748, Jun. 2018.
[34] F. Zhao, D. Inserra, G. Wen, J. Li, and Y. Huang, "A high-efficiency inverse class-F microwave rectifier for wireless power transmission," *IEEE Microw. Wireless Compon. Lett.*, vol. 29, no. 11, pp. 725–728, Nov. 2019.
[35] T. Ngo and Y.-X. Guo, "Harmonic-recycling rectifier for high-efficiency far-field wireless power transfer," *IEEE Trans. Circuits Syst. II, Exp. Briefs*, vol. 67, no. 4, pp. 770–774, Apr. 2020.
[36] F. H. Raab, "Class-E, class-C, and class-F power amplifiers based upon a finite number of harmonics," *IEEE Trans. Microw. Theory Techn.*, vol. 49, no. 8, pp. 1462–1468, Aug. 2001.

DANH MANH NGUYEN (Student Member, IEEE) received the B.Sc. (Eng.) degree in electronics and telecommunication from the School of Electronics and Telecommunication (SET), Hanoi University of Science and Technology, Hanoi, Vietnam, in 2020. He is currently pursuing the M.Sc. degree with the Department of Information Communication, Materials, and Chemistry Convergence Technology, Soongsil University, Seoul, South Korea.

His research interests include high gain antenna, wideband antennas, multilple-polarized antennas, wireless power transfer, and metamaterials.

NGOC DUC AU (Member, IEEE) received the B.S. degree in electronics and telecommunications from Vietnam National University Ho Chi Minh City University of Science, Ho Chi Minh, Vietnam, in 2011, and the Ph.D. degree in information and telecommunication engineering from Soongsil University, Seoul, South Korea, in 2020.

He was a Senior Researcher with the National Key Laboratory of Digital Control and System Engineering, Ho Chi Minh, until 2015. He is currently a Postdoctoral Researcher with Soongsil University. His current research interests include microwave wireless power transfer, solar space power satellite, microwave power amplifier, microwave rectifier, non-foster circuit, and RFIC.

CHULHUN SEO (Senior Member, IEEE) received the B.S., M.S., and Ph.D. degrees from Seoul National University, Seoul, South Korea, in 1983, 1985, and 1993, respectively. From 1993 to 1995, he worked with Massachusetts Institute of Technology (MIT), Cambridge, MA, USA, as a Technical Staff Member. From 1993 to 1997, he worked as an Assistant Professor with Soongsil University, Seoul. From 1999 to 2001, he was a Visiting Professor with MIT. From 1997 to 2004, he was an Assistant Professor with Soongsil University, where he has been a Professor of electronic engineering, since 2004. He is currently the Director of the Wireless Power Transfer Research Center supported by the Korean Ministry of Trade, Industry, and Energy, and the Metamaterials Research Center, which is supported by the Basic Research Laboratories through the NRF Grant funded by the MSIP. His research interests include wireless communication technologies, RF power amplifiers, and wireless power transfer using meta-materials. He served as the IEEE MTT Korea Chapter Chairperson, from 2011 to 2014.